Supporting Information for "A long-lived sharp disruption on the lower clouds of Venus"

DOI: 10.1029/2020GL087221

J. Peralta[1], T. Navarro[2,3,4], C. W. Vun[1], A. Sánchez-Lavega[5], K. McGouldrick[6], T. Horinouchi[7], T. Imamura[8], R. Hueso[5], J. P. Boyd[9], G. Schubert[2], T. Kouyama[10], T. Satoh[1], N. Iwagami[11], E. F. Young[12], M. A. Bullock[12], P. Machado[13], Y. J. Lee[14], S.S. Limaye[15], M. Nakamura[1], S. Tellmann[16], A. Wesley[17]and P. Miles[18]

[1]Institute of Space and Astronautical Science, JAXA, Sagamihara, Japan.
[2]Department of Earth, Planetary, and Space Sciences, University of California, Los Angeles, CA, USA.
[3]McGill Space Institute, McGill University, Montréal, QC, Canada.
[4]Department of Earth and Planetary Sciences, McGill University, Montréal, QC, Canada.
[5]Escuela de Ingeniería de Bilbao, UPV/EHU, Bilbao, Spain.
[6]Laboratory for Atmospheric and Space Physics, Univ. of Colorado Boulder, Boulder, CO, USA.
[7]Faculty of Environmental Earth Science, Hokkaido University, Hokkaido, Japan.
[8]Graduate School of Frontier Sciences, The University of Tokyo, Tokyo, Japan.
[9]CLaSP Department, University of Michigan College of Engineering, Ann Arbor, USA.
[10]Artificial Intelligence Research Center, National Institute of Advanced Industrial Science and Technology, Japan.
[11]Tokyo 156-0044, Japan.
[12]Southwest Research Institute, Boulder, CO 80302, USA.
[13]Institute of Astrophysics and Space Sciences, Portugal.
[14]Technische Universität Berlin, Berlin, Germany.
[15]Space Science and Engineering Center, University of Wisconsin, Madison, WI, USA.
[16]Abteilung Planetenforschung, Rheinisches Institut für Umweltforschung, Universität zu Köln, Cologne, Germany.
[17]Astronomical Society of Australia, Murrumbateman, New South Wales, Australia.
[18]Gemeye Observatory, Rubyvale, Queensland, Australia.

Contents of this file

1. Figures S1 to S6
2. Tables S1 and S2

Additional Supporting Information (Files uploaded separately)

1. Description of Dataset S1
2. Descriptions of Movies S1 and S2

Introduction. This Supporting Information document contains additional Figures, Tables and the caption of the Movies supporting the conclusions of this work. Figure S1 exhibits the statistics for atmospheric temperature, pressure and number density as measured on the nightside of Venus during with radio-occultation data during 2006–2016 from Venus Express and Akatsuki. Figure S2 displays all the cases of clouds' disruption identified in images of Venus's day (900 nm) and night side (2.26 μm) obtained by the cameras IR1 and IR2 (Iwagami et al., 2018; Satoh et al., 2017) onboard JAXA's orbiter Akatsuki (Nakamura et al., 2016). Figure S3 reproduces the same sample of Venus images presented in Fig. S2 but projected onto equirectangular geometry. Figure S4 presents more examples of the disruption as observed with ground-based observations and with the imaging spectrometer VIRTIS-M onboard the Venus Express mission (Drossart et al., 2007). Figure S5 explores whether the morphology and orientation of the disruption is related to the surface elevations at the location of the subsolar point. Figure S6 displays the Kelvin wave disturbances when the mountain wave parameterization is activated in the IPSL Venus GCM (Lebonnois et al., 2010, 2016; Garate-Lopez & Lebonnois, 2018). Also, Table S1 exhibits information about the imagery data set used in this work, while Table S2 gives detailed information about the decrease of the West-to-East radiance across identified disruption events on the lower clouds during the Venus Express mission. Finally, we also included descriptions of the Supplementary Dataset S1 and Supplementary Movies S1 and S2 (uploaded separately).

0094-8276/20/$5.00

Figure S1.

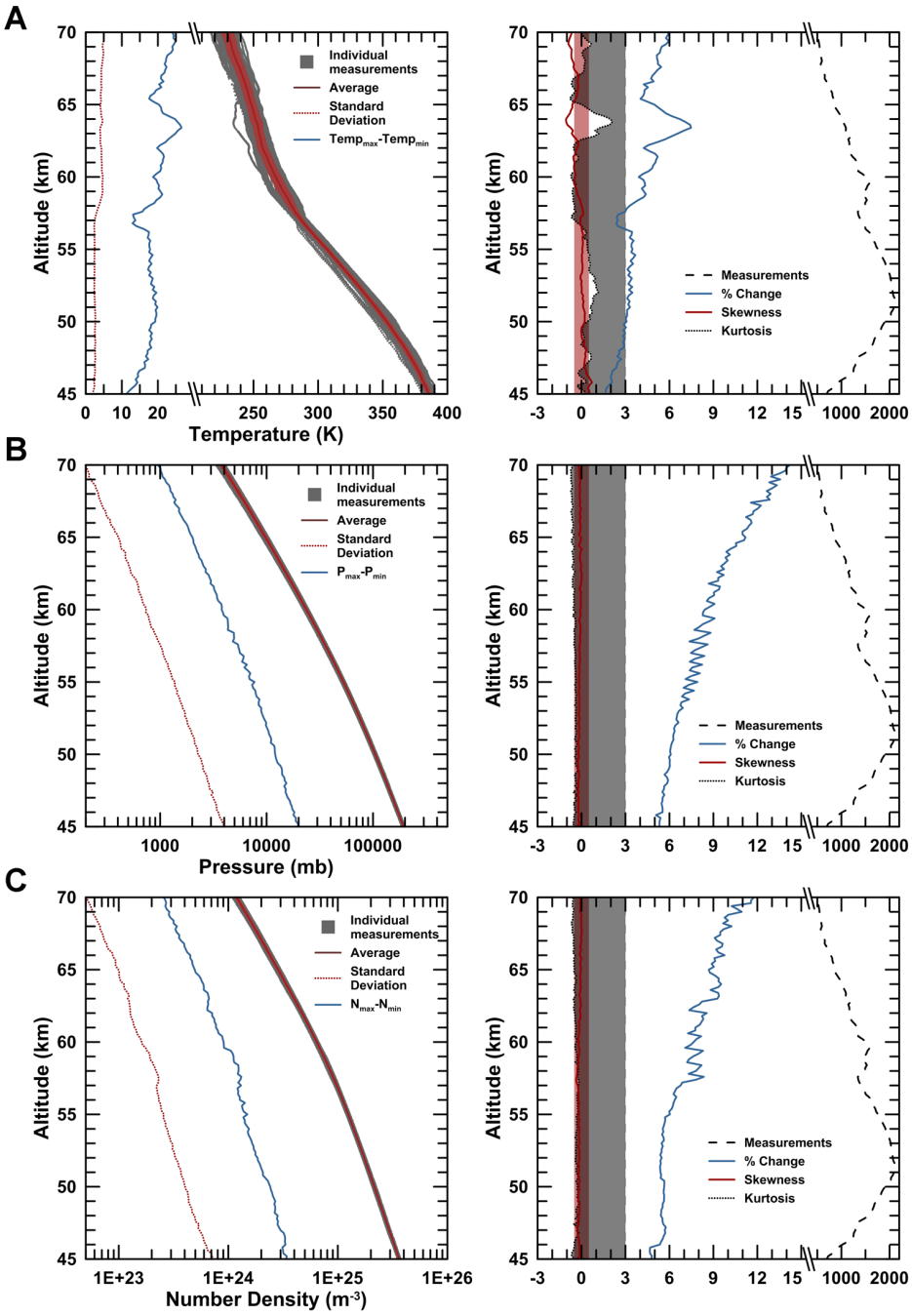

Figure S1. Atmospheric parameters on the night of Venus from radio-occultation measurements. Vertical profiles of the night temperature (A), pressure (B) and number density (C) from 85 radio-occultation profiles within 30°N–30°S and during 2006–2016 by Venus Express and Akatsuki. Vertical bins of 200 m were used for calculations. In right column: percent of change for the maximum deviation (relative to the mean), Skewness, Kurtosis and number of measurements within each vertical bin. The dark red area stands for symmetric data limited by Skewness values -0.5 and +0.5. The grey area stands for Kurtosis lower than 3 (no heavy tails or outliers).

Figure S2.

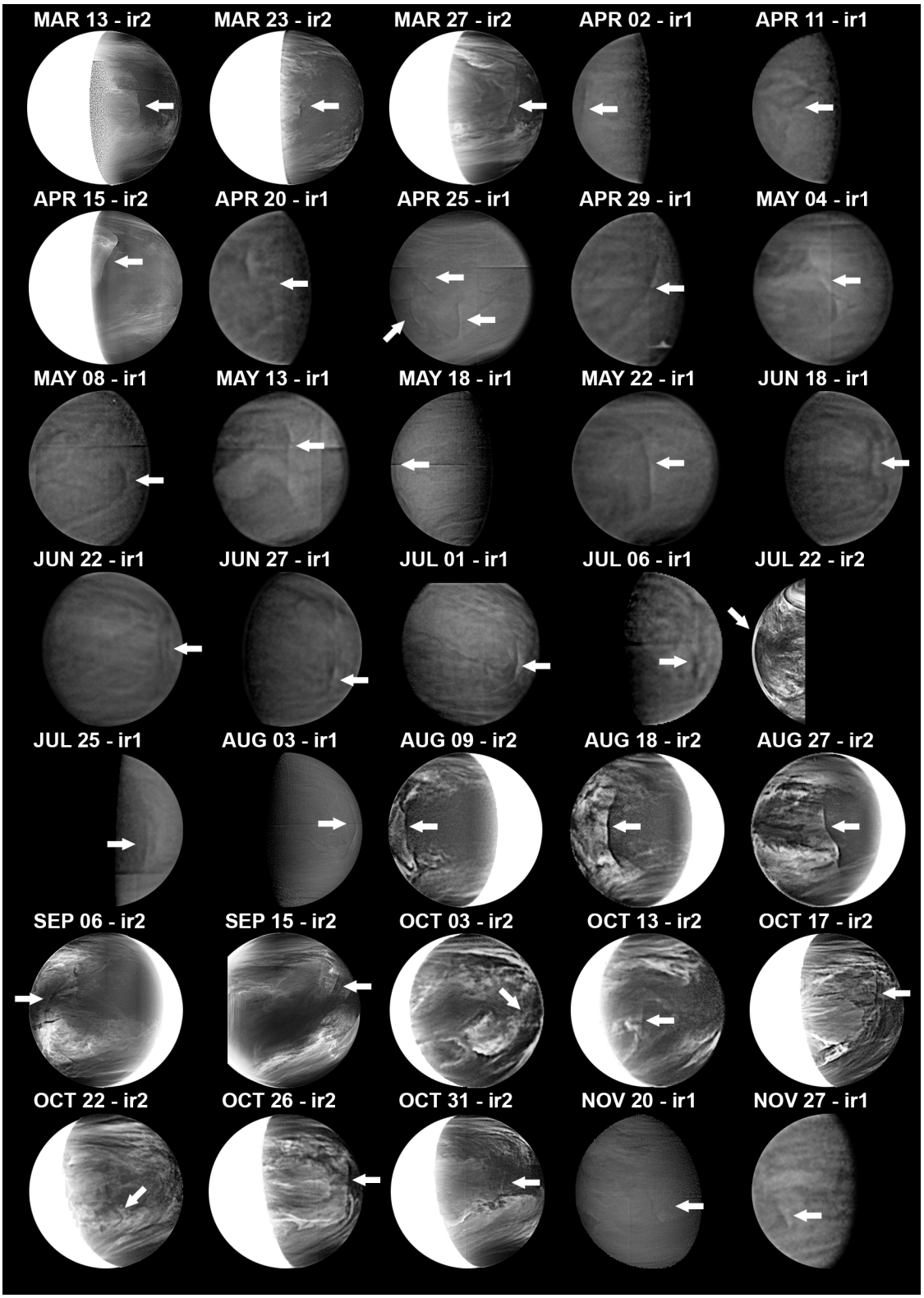

Figure S2. Akatsuki observations of the clouds' disruption during 2016. IR2/2.26-μm (nightside clouds' opacity) and IR1/900-nm images (dayside albedo) are displayed. The images were processed as described in the main work. Events of the disruption were identified in the next dates of the year 2016: 13, 23 and 27 of March; 2, 11, 15, 20, 25 and 29 of April; 4, 8, 13, 18 and 22 of May; 18, 22 and 27 of June; 1, 6, 22 and 25 of July; 3, 9, 18 and 27 of August; 6 and 15 of September; 3, 13, 17, 22, 26 and 31 of October; 20 and 27 of November.

Figure S3.

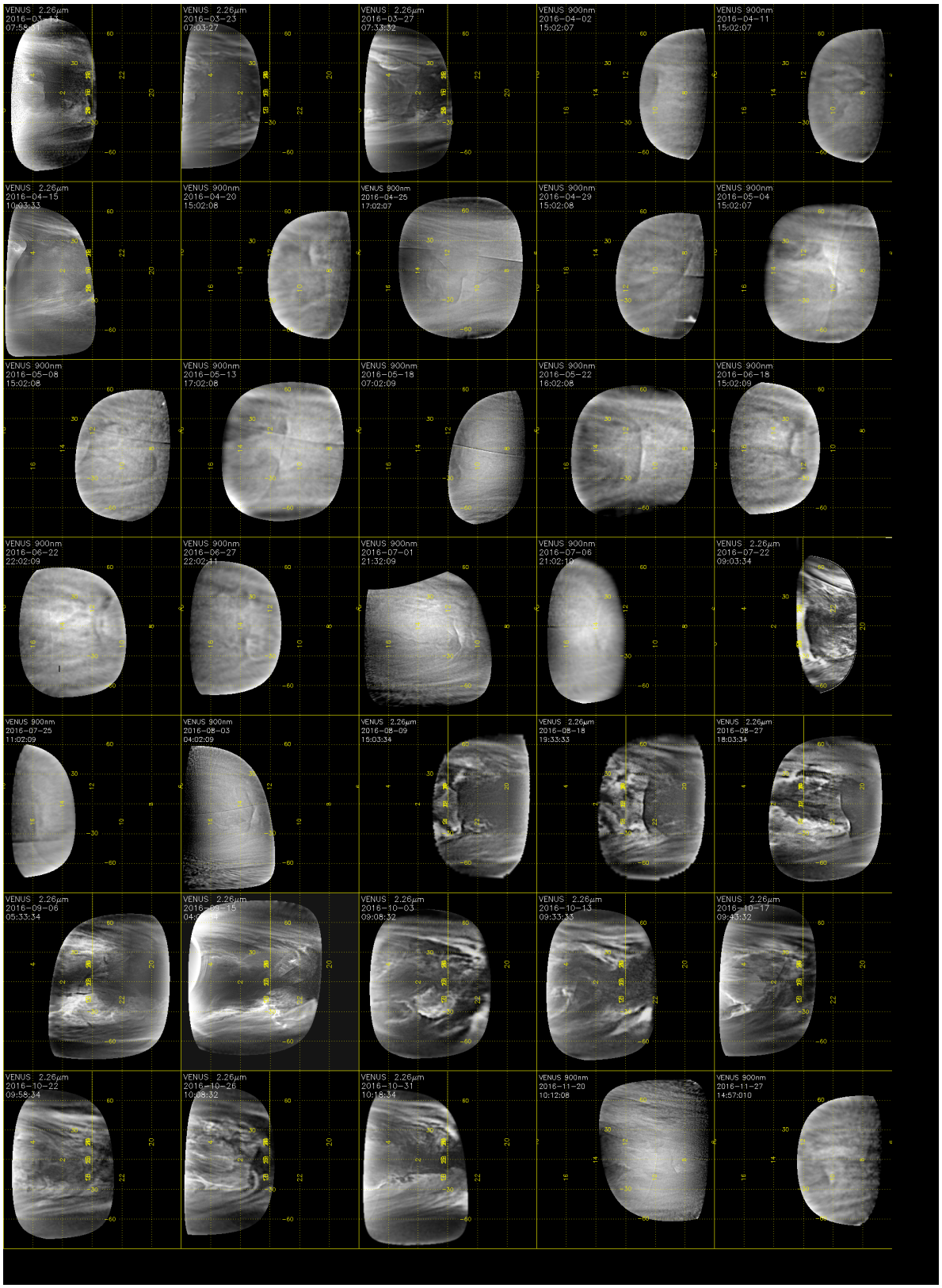

Figure S3. Cylindrical projections of Akatsuki observations of the cloud disruption during 2016. Contents are the same as in Extended Figure 1 although with the Akatsuki images displayed as equirectangular projections with grid resolution of 0.5° per pixel and latitude and local time boundaries 90°N–90°S and 06h–18h (dayside) and 18h–06h (nightside). The dates and times for each image are displayed at the left-up corner or each projection.

Figure S4.

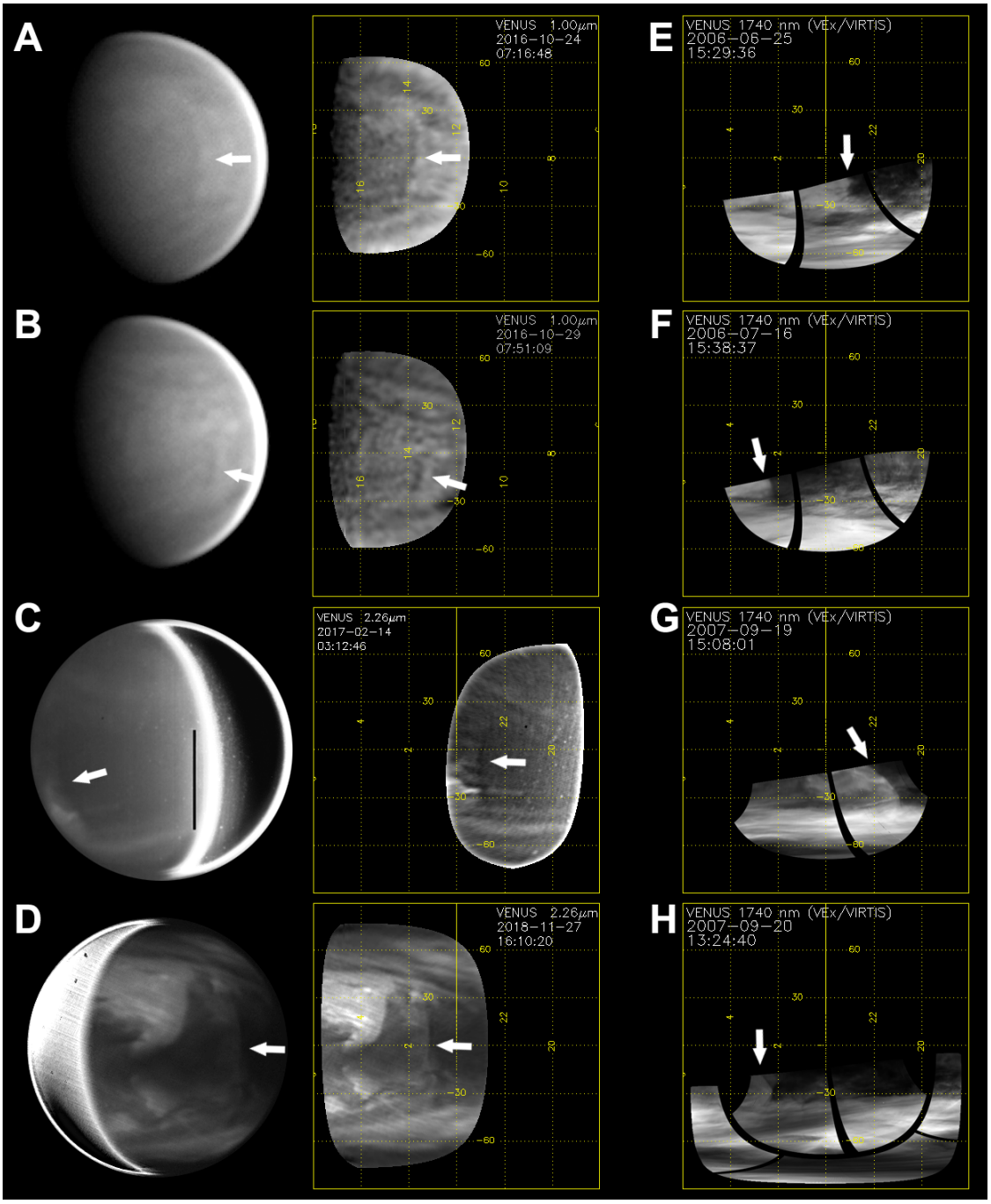

Figure S4. The cloud disruption with ground-based observations and Venus Express. The disruption was also identified in images of the dayside of Venus taken at 1 μm with small telescopes by observers P. Miles and A. Wesley (A–B) and on images of the nightside acquired with IRTF/SpeX using a K_{cont} filter (C–D) and with VEx/VIRTIS-M at 1.74 μm (E–H). The cylindrical projections were made for the full dayside or nightside and with a spatial resolution of 0.5° per pixel.

Figure S5.

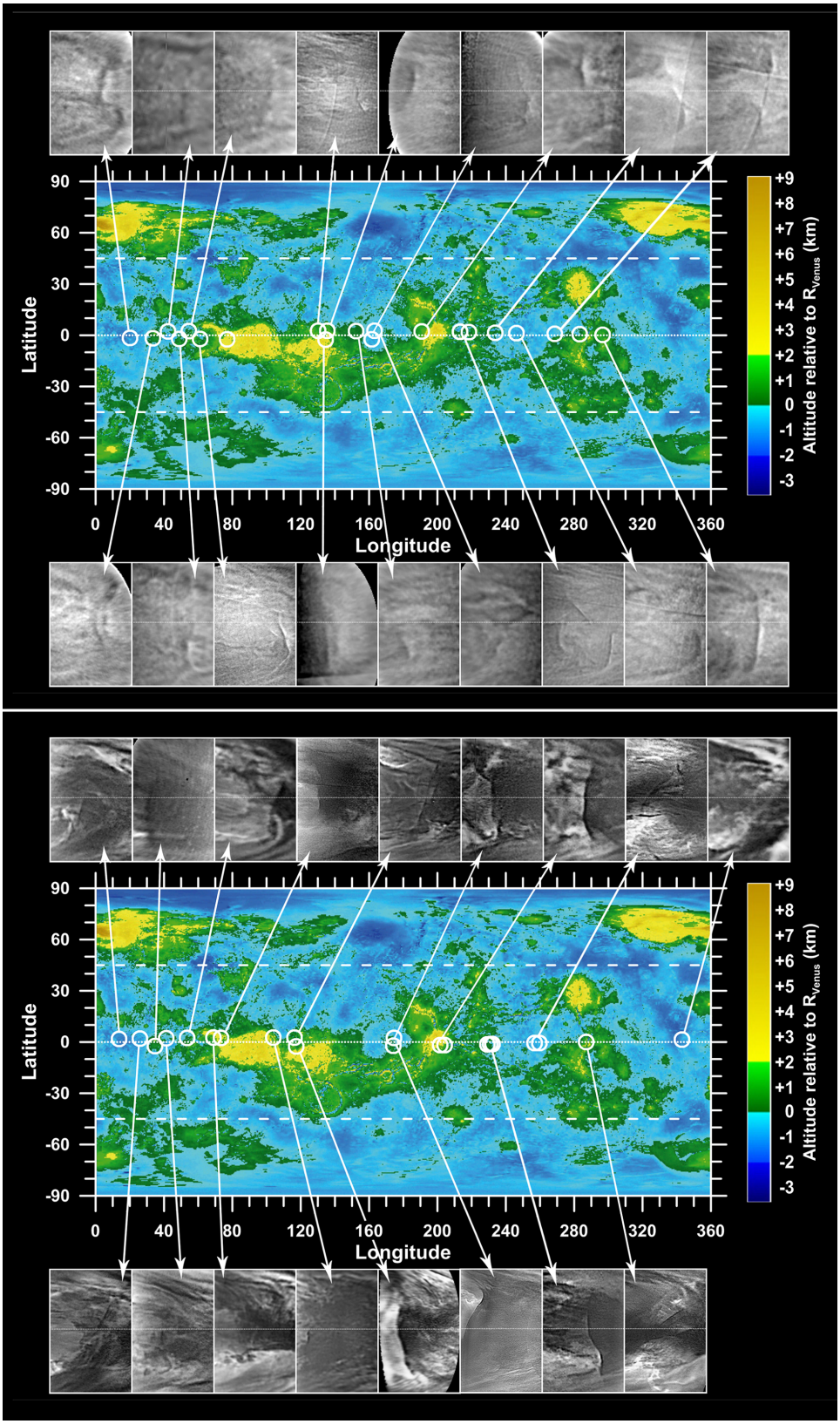

Figure S5. Comparison of the cloud morphology and surface topography. The morphology of the disruption in IR1/900-nm images (graph above) and IR2/2.26-μm images (graph below) is compared with the geographical location of the subsolar point during the observations (white circle). The disruptions are shown as cylindrical projections (45°N–45°S and longitude width of 60°). Latitudes 0° and 45° are marked with white dotted and dashed lines, respectively. Disruptions' morphology and hemispherical asymmetry seems unrelated to the surface elevations at the subsolar point, what might rule out the geographical location of the maximum solar heating as a probable excitation source of the disruption.

Figure S6.

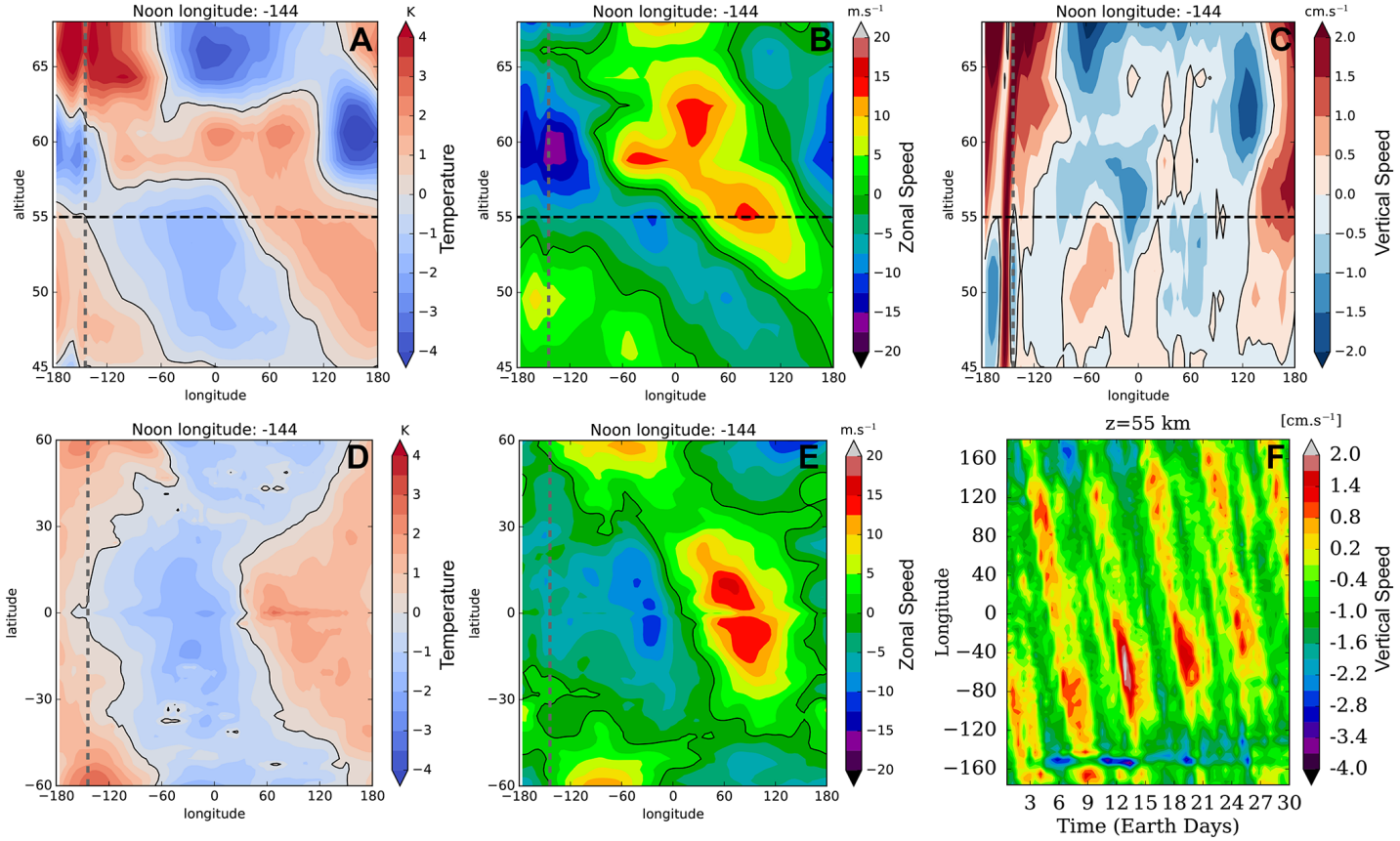

Figure S6. Kelvin wave according to the IPSL Venus GCM: mountain wave parameterization activated. Similarly to Figure 4 in the main article, the disturbances for the temperature, zonal and vertical speeds are shown as the vertical cross-sections within 45–68 km (A–C), while disturbances for the temperature and zonal speeds are displayed with the horizontal cross-section at 55 km height (D–E). A Hovmöller diagram for the vertical speed is also shown (F). Noon longitude and 55-km altitude level over the surface are shown with grey and black dashed lines, respectively. The mountain wave is set at longitude -160. In our simulations, the Kelvin wave is observed to pass through the mountain wave 3 Earth days later with minimal effect on the zonal wind speeds.

Table S1.

Cloud level sensed	Mission/ Instrument	Wavelength (μm)	Images inspected	Time coverage	Days covered	Disruption cases
Night side Lower Clouds	VEx/VIRTIS	1.74	4118	from April 2006 to October 2008	376	12
”	Akatsuki/IR2	2.26	238	from March 2016 to November 2016	68	16
”	IRTF/SpeX	2.32	62	from January 2017 to December 2018	31	5
”	IRTF/iSHELL	2.32	16	from January 2017 to December 2018	8	2
Day side Middle Clouds	Akatsuki/IR1	0.90	984	from December 2015 to December 2016	173	19
”	Small Telescope	1.0-1.1	19	from October 2016 to November 2016	13	2

Table S1. Summary of imagery data set used in this work. The dayside middle clouds are located within 50.5–56.5 km, while the nightside lower clouds are within 47.5–50.5 km (Titov et al., 2018).

Table S2.

VIRTIS Cube	Date (yyyy-mm-dd)	Time (hh:mm:ss)	Wavelength (μm)	Radiance on West (W/m^2/sr/μm)	Radiance on East (W/m^2/sr/μm)	Radiance Decrease
VI0066_01	2006-06-25	15:29:36	1.74	0.07441	0.0179	76%
”	”	”	2.26	0.02403	0.001527	94%
”	”	”	2.32	0.009926	0.0009053	91%
VI0087_00	2006-07-16	15:10:37	1.74	0.06815	0.02117	69%
”	”	”	2.26	0.02701	0.003897	86%
”	”	”	2.32	0.008268	0.001345	84%
VI0111_04	2006-08-09	18:34:48	1.74	0.06708	0.00839	88%
”	”	”	2.26	0.01701	0.0008601	95%
”	”	”	2.32	0.003388	0.0003588	89%
VI0121_11	2006-08-19	22:19:47	1.74	0.06649	0.01491	78%
”	”	”	2.26	0.01701	0.004111	76%
”	”	”	2.32	0.006748	0.001426	79%
VI0159_00	2006-09-26	18:40:37	1.74	0.05589	0.01851	67%
”	”	”	2.26	0.01475	0.001605	89%
”	”	”	2.32	0.01247	0.0007836	94%
VI0218_06	2006-11-24	18:34:31	1.74	0.07565	0.01687	78%
”	”	”	2.26	0.01983	0.001339	93%
”	”	”	2.32	0.007337	0.000382	95%
VI0517_01	2007-09-19	15:08:01	1.74	0.1117	0.03523	69%
”	”	”	2.26	0.04477	0.00683	85%
”	”	”	2.32	0.01805	0.002687	85%

Table S2. Decrease of the Radiance across the Disruption. The West-to-East decrease of the night side lower clouds' radiance across the disruption has been characterized for 7 cubes of the VEx/VIRTIS data set. Measurements were made for images at three wavelengths: 1.74, 2.26 and 2.32 μm.

Data Set S1. Simulation with the IPSL Venus GCM. The compressed zip file accompanying this article (https://zenodo.org/record/3817479) holds a NetCDF file with a README file describing its structure. The NetCDF file contains the IPSL GCM simulation of the Venus atmosphere for the case of a relaxed zonal wind profile (see subsection 2.4 in main article). Computations were performed on a grid of altitude×latitude×longitude with 50×97×96 elements and along 40 time steps covering 23 Earth days. Calculated physical parameters include:

1. Atmospheric pressure (Pa).
2. Vertical Wind ($m \cdot s^{-1}$) [positive downward].
3. Air Temperature (K).
4. Zonal Wind ($m \cdot s^{-1}$) [positive westward].
5. Solar radiance at top of the atmosphere ($W \cdot m^{-2}$).

Movie S1. Animated Time Composites of the lower clouds of Venus during 10–16 of October 2016 and 1–10 of December 2018. This animated GIF file displays satellite projections of the time series of the nightside lower clouds of Venus shown in Figures 1C and 1D in the main article. The first time series was constructed with 2.26-μm images obtained by the IR2 camera onboard JAXA's orbiter, and compress dates from 10 to 16 of October 2016. The second time series was made with images from ground-based observations by the instrument SpeX at NASA's IRTF infrared telescope. Before being combined to construct the time series, all the individual images were projected onto equirectangular geometry between 60°N–60°S and with a resolution of 0.5° per pixel. The satellite projections are centred at 0° latitude (equator) and 00:00 local time (midnight).

Movie S2. The lower clouds of Venus during 15–30 of August 2016. This animated GIF file displays two full cycles of the nightside lower clouds of Venus as observed at 2.26 μm by the IR2 camera onboard JAXA's orbiter Akatsuki. The passage of the equatorial cloud disruption can be observed during August 18–19 and 27–28. The images were processed to highlight finer cloud patterns (see Methods section in main article) and projected onto a satellite geometry centered at 0° latitude (equator) and 00:00 local time (midnight). Latitudes 60°N, 30°N, 0°, 30°S and 60°S are displayed with dotted lines. Although the image processing highly reduces the problem of the light contamination in the IR2 images (Satoh et al., 2017), its effect is yet apparent in this animation.

References

Drossart, P., Piccioni, G., Adriani, A., Angrilli, F., Arnold, G., Baines, K. H., ... Afanasenko, T. Z. (2007, October). Scientific goals for the observation of Venus by VIRTIS on ESA/Venus express mission. *Planetary and Space Science*, *55*, 1653-1672. doi: 10.1016/j.pss.2007.01.003

Garate-Lopez, I., & Lebonnois, S. (2018, Nov). Latitudinal variation of clouds' structure responsible for Venus' cold collar. *Icarus*, *314*, 1-11. doi: 10.1016/j.icarus.2018.05.011

Iwagami, N., Sakanoi, T., Hashimoto, G. L., Sawai, K., Ohtsuki, S., Takagi, S., ... Kouyama, T. (2018, January). Initial products of Akatsuki 1-μm camera. *Earth, Planets, and Space*, *70*, 6. doi: 10.1186/s40623-017-0773-5

Lebonnois, S., Hourdin, F., Eymet, V., Crespin, A., Fournier, R., & Forget, F. (2010, June). Superrotation of Venus' atmosphere analyzed with a full general circulation model. *Journal of Geophysical Research (Planets)*, *115*, E06006. doi: 10.1029/2009JE003458

Lebonnois, S., Sugimoto, N., & Gilli, G. (2016). Wave analysis in the atmosphere of Venus below 100-km altitude, simulated by the LMD Venus GCM. *Icarus*, *278*, 38–51. Retrieved from `http://www.sciencedirect.com/science/article/pii/S0019103516302688` doi: 10.1016/j.icarus.2016.06.004

Nakamura, M., Imamura, T., Ishii, N., Abe, T., Kawakatsu, Y., Hirose, C., ... Kamata, Y. (2016). AKATSUKI returns to Venus. *Earth, Planets and Space*, *68*(1), 1-10. Retrieved from `http://dx.doi.org/10.1186/s40623-016-0457-6` doi: 10.1186/s40623-016-0457-6

Satoh, T., Sato, T. M., Nakamura, M., Kasaba, Y., Ueno, M., Suzuki, M., ... Ohtsuki, S. (2017, November). Performance of Akatsuki/IR2 in Venus orbit: the first year. *Earth, Planets, and Space*, *69*, 154. doi: 10.1186/s40623-017-0736-x

Titov, D. V., Ignatiev, N. I., McGouldrick, K., Wilquet, V., & Wilson, C. F. (2018, Dec). Clouds and Hazes of Venus. *Space Science Reviews*, *214*(8), 126. doi: 10.1007/s11214-018-0552-z